
# NAVAL POSTGRADUATE SCHOOL

**MONTEREY, CALIFORNIA**

# THESIS

**NOVEL NANOMATERIAL-PARAFFIN-EPOXY PHASE-CHANGE MATERIAL FORMULATIONS**

by

Joshua A. Hanna

June 2019

| | |
|---|---|
| Thesis Advisor: | Claudia C. Luhrs |
| Second Reader: | Troy Ansell |

THIS PAGE INTENTIONALLY LEFT BLANK

| REPORT DOCUMENTATION PAGE | *Form Approved OMB No. 0704-0188* |
|---|---|



| **1. AGENCY USE ONLY** *(Leave blank)* | **2. REPORT DATE** June 2019 | **3. REPORT TYPE AND DATES COVERED** Master's thesis |
|---|---|---|

**4. TITLE AND SUBTITLE**
NOVEL NANOMATERIAL-PARAFFIN-EPOXY PHASE-CHANGE MATERIAL FORMULATIONS

**5. FUNDING NUMBERS**

**6. AUTHOR(S)** Joshua A. Hanna

**7. PERFORMING ORGANIZATION NAME(S) AND ADDRESS(ES)**
Naval Postgraduate School
Monterey, CA 93943-5000

**8. PERFORMING ORGANIZATION REPORT NUMBER**

**9. SPONSORING / MONITORING AGENCY NAME(S) AND ADDRESS(ES)**
Office of Naval Research, Arlington, VA 22203

**10. SPONSORING / MONITORING AGENCY REPORT NUMBER**

**11. SUPPLEMENTARY NOTES** The views expressed in this thesis are those of the author and do not reflect the official policy or position of the Department of Defense or the U.S. Government.

**12a. DISTRIBUTION / AVAILABILITY STATEMENT**
Approved for public release. Distribution is unlimited.

**12b. DISTRIBUTION CODE**
A

**13. ABSTRACT (maximum 200 words)**

The regulation of temperature within living and storage spaces in high-temperature environments is a demanding challenge mostly met using high-fuel consuming air conditioning systems. Phase-change material (PCM) systems have the potential to decrease military operating costs and ease operating demands. By passively regulating temperature cycles through absorbing heat during daytime and releasing heat during nighttime, PCM systems can decrease the need for conventional air conditioning systems. The aim of this research was to encapsulate a PCM into an epoxy resin, which would be applied to fabric for use as a lining in living or storage spaces. Nonadecane, an organic hydrocarbon with a melting temperature of 32°C and sufficient cyclability, was selected as a suitable PCM material. The epoxy-PCM composite was manufactured using the thickening agent Carbopol to aid in the emulsification of PCM and epoxy. Various micro- and nano-scale thermally conductive additives were included into the composite formulations to improve thermal performance. Using 3D printing strategies, the new epoxy-PCM composite system was successfully attached to fabric to create a removable liner.

| **14. SUBJECT TERMS** phase change material, nanomaterial, energy storage | **15. NUMBER OF PAGES** 63 |
|---|---|
| | **16. PRICE CODE** |

| **17. SECURITY CLASSIFICATION OF REPORT** | **18. SECURITY CLASSIFICATION OF THIS PAGE** | **19. SECURITY CLASSIFICATION OF ABSTRACT** | **20. LIMITATION OF ABSTRACT** |
|---|---|---|---|
| Unclassified | Unclassified | Unclassified | UU |

NSN 7540-01-280-5500

Standard Form 298 (Rev. 2-89)
Prescribed by ANSI Std. 239-18

THIS PAGE INTENTIONALLY LEFT BLANK

**Approved for public release. Distribution is unlimited.**

# NOVEL NANOMATERIAL-PARAFFIN-EPOXY PHASE-CHANGE MATERIAL FORMULATIONS

Joshua A. Hanna
Ensign, United States Navy
BS, U.S. Naval Academy, 2018

Submitted in partial fulfillment of the
requirements for the degree of

**MASTER OF SCIENCE IN MECHANICAL ENGINEERING**

from the

**NAVAL POSTGRADUATE SCHOOL**
**June 2019**

Approved by: Claudia C. Luhrs
Advisor

Troy Ansell
Second Reader

Garth V. Hobson
Chair, Department of Mechanical and Aerospace Engineering

THIS PAGE INTENTIONALLY LEFT BLANK

# ABSTRACT

The regulation of temperature within living and storage spaces in high-temperature environments is a demanding challenge mostly met using high-fuel consuming air conditioning systems. Phase-change material (PCM) systems have the potential to decrease military operating costs and ease operating demands. By passively regulating temperature cycles through absorbing heat during daytime and releasing heat during nighttime, PCM systems can decrease the need for conventional air conditioning systems. The aim of this research was to encapsulate a PCM into an epoxy resin, which would be applied to fabric for use as a lining in living or storage spaces. Nonadecane, an organic hydrocarbon with a melting temperature of 32°C and sufficient cyclability, was selected as a suitable PCM material. The epoxy-PCM composite was manufactured using the thickening agent Carbopol to aid in the emulsification of PCM and epoxy. Various micro- and nano-scale thermally conductive additives were included into the composite formulations to improve thermal performance. Using 3D printing strategies, the new epoxy-PCM composite system was successfully attached to fabric to create a removable liner.

THIS PAGE INTENTIONALLY LEFT BLANK

# TABLE OF CONTENTS

THIS PAGE INTENTIONALLY LEFT BLANK

# LIST OF FIGURES

# LIST OF TABLES

THIS PAGE INTENTIONALLY LEFT BLANK

# LIST OF ACRONYMS AND ABBREVIATIONS

| | |
|---|---|
| B | boron |
| BN | boron nitride |
| BNNT | boron nitride nanotube |
| C | carbon |
| CNF | carbon nanofiber |
| CNT | carbon nanotube |
| cm | centimeter |
| cP | centipoise |
| DSC | differential scanning calorimetry |
| EC | epoxy-carbopol 5wt% |
| μm | micrometer |
| mm | millimeter |
| N | nitrogen |
| nm | nanometer |
| NPS | Naval Postgraduate School |
| PCM | phase change materials |
| psig | pounds per square inch gauge |
| Pt/Pd | platinum/palladium |
| rpm | revolution per minute |
| SEM | scanning electron microscope |
| SiC | silicon carbide |
| TAL | Thermal Analysis Labs |
| TES | thermal energy storage |
| TGA | thermogravimetric analysis |
| XRD | X-ray diffractometer |

THIS PAGE INTENTIONALLY LEFT BLANK

# ACKNOWLEDGMENTS

I would like to thank Claudia Luhrs for her support as my thesis advisor. She has expertly guided me through every step of my graduate-level work while also allowing for me to take ownership of my thesis. I have greatly enjoyed studying my thesis topic, and I appreciate her providing the direction to make it successful. She constantly made herself available to assist me, and she has ensured that my graduate studies have been worthwhile.

I also want to thank Richa Agrawal for her invaluable assistance throughout the fabrication and characterization processes. She quickly familiarized herself with the project and immediately provided her support. Her technical expertise greatly contributed to the success of this project.

I also want to thank Troy Ansell for his role as the second reader of my thesis and for instructing me on the operation of the SEM. His review ensured the best version of my work will be presented.

Additionally, I would like to thank Sarath Menon and Chanman Park for their assistance throughout the characterization process. They are continuously working to support many projects, and I appreciate the time they spent to assist me.

Finally, I am lucky to have to have the constant support of my loving wife, Jamie. She has encouraged me to succeed throughout my life, and I am grateful for all she does for me. I would also like to thank my two loving dogs, Eevee and Appa, for hanging out with me during many late nights in my office.

THIS PAGE INTENTIONALLY LEFT BLANK

# I. INTRODUCTION

## A. MILITARY MOTIVATION

The regulation of temperature within enclosed living and storage spaces has been and will be a continuing challenge for the United States military. The expeditionary nature of many conflicts requires the military to operate far from the mainland United States and far from potentially supportive allies. The military must transport large amount of materials and expend a huge amount of energy to conduct these operations [1]. Any potential method to decrease the energy burden associated with these operations could provide large monetary and operational benefits. High temperature climates are one particularly demanding environment in which the U.S. military has operated continuously for over a decade, and will likely continue to operate, for the foreseeable future [2].

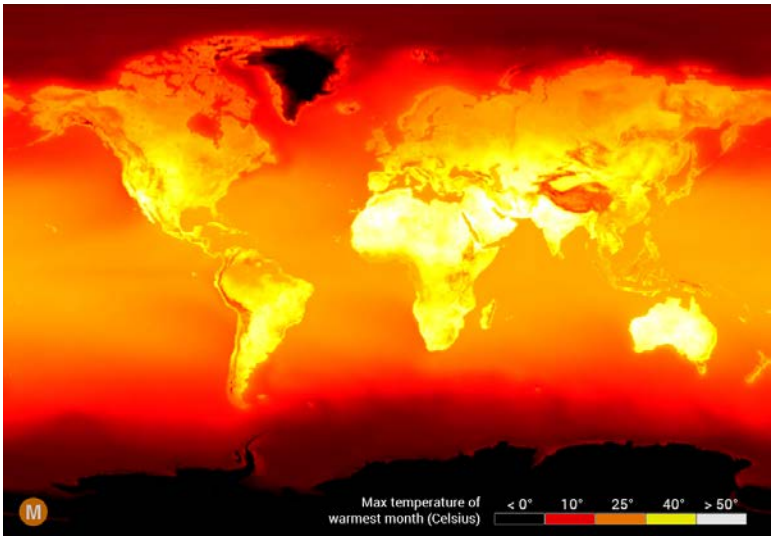


Figure 1. Global maximum recorded temperatures. Source: [3].

Figure 1 is a visualization of areas of the world with high temperature environments. The colors correspond to the maximum temperature recorded from 2000–2009 [3]. It shows that large areas of the globe can reach above 30 $^{o}$C in the warmest months of the year. The maximum recorded temperature is an important figure, but a more realistic visualization of a location's climate is provided by a graph of daily maximum and

minimum temperatures. Figure 2 shows such a graph for two locations with peak yearly temperatures of ~50 $^{o}$C [4], [5].

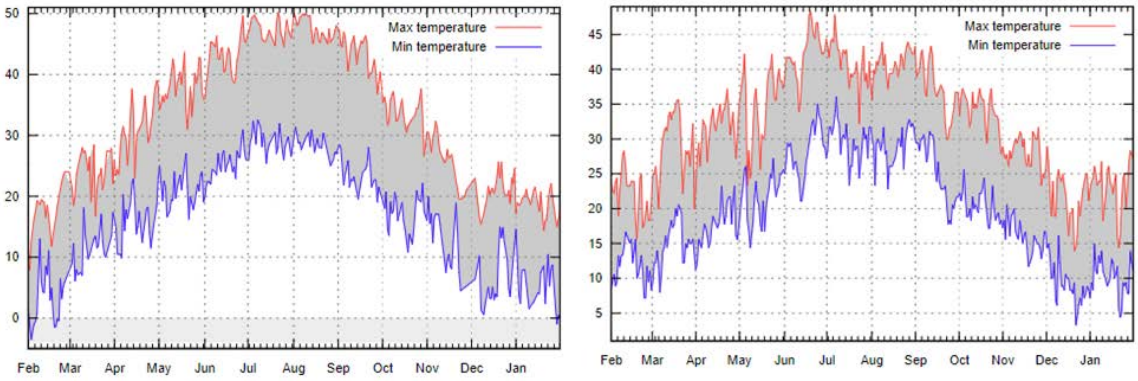


Temperatures given from February 2017 to January 2018.

Figure 2. Daily temperatures of Baghdad (left) and Phoenix (right). Adapted from [4],[5].

These two graphs reflect a better representation of the daily temperature fluctuations of a location. The inclusion of the minimum daily temperature shows an important consideration for the harshness of an environment. The natural daily temperature cycle can be used to help mitigate the peak temperature during the day. The peak daytime temperature may reach up to 50 $^{o}$C, but the nighttime temperature can drop to 30 $^{o}$C or below. This temperature difference can be harnessed to help regulate daytime extremes.

Another important consideration is the effect of solar radiation on the amount of heat imparted on a surface. Figures 1 and 2 show data for air temperatures measured under the shade. Surfaces exposed to the sun can rise to temperatures above the temperature of the air due to the heat of the solar radiation. Radiation flux on a day with a clear sky can be as high as 1000 W/m$^2$ [6]. The heating difference between the sun and shade can also be used to help thermal regulation.

## B. THERMAL ENERGY STORAGE

Thermal energy storage (TES) systems take advantage of thermal gradients to absorb excess energy to be released at a later time. This storage ability can be used for a

variety of applications, such as storage of excess renewable energy generated during off peak times. Figure 3 details the various categories of thermal energy storage systems.

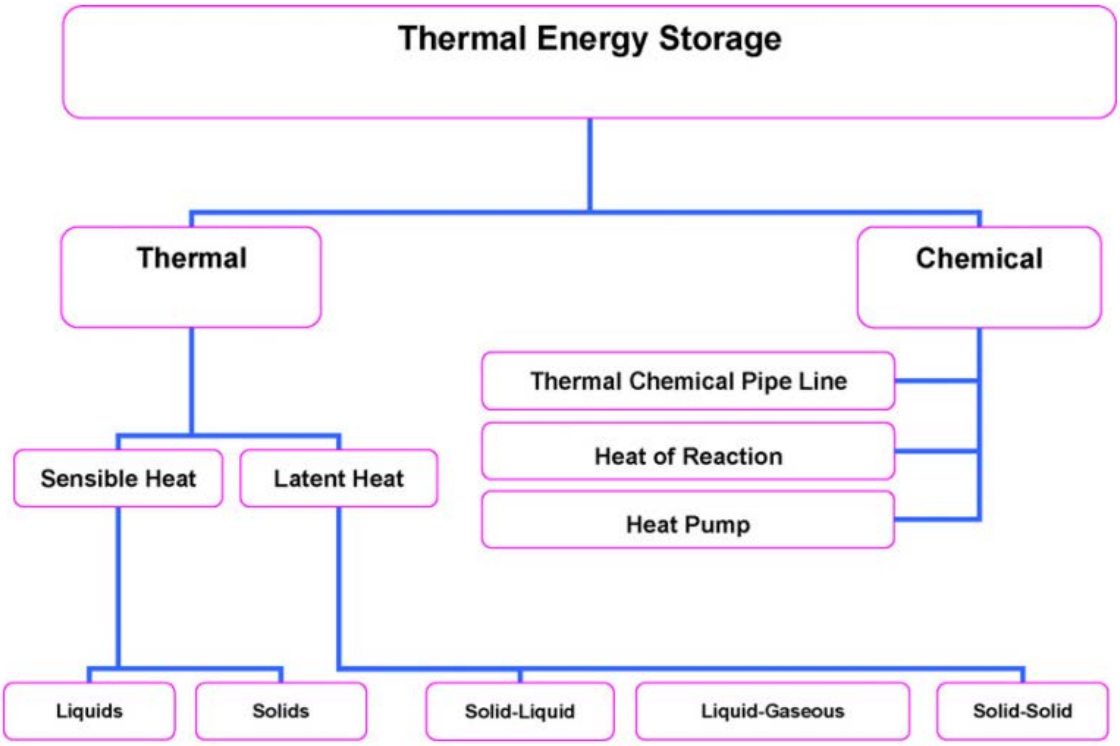


Figure 3. Breakdown of TES categories. Source: [7].

TES systems can be divided into two major categories, thermal and chemical. Chemical TES systems uses the excess heat to drive a chemical reaction. The products of this reaction can then be stored as a source of potential energy. Thermal TES systems transfers the excess heat to another material. This heat transfer can occur through two processes, sensible or latent. Sensible heat transfer increases the temperature of the transfer material as heat is applied. The use of waste heat to increase the temperature of underground water and rock beds is a commonly used sensible TES [8]. Latent heat transfer does not increase the temperature of the transfer material, the heat instead causes the material to undergo a phase change. This phase change is most commonly a solid-liquid transition. Materials with high latent heat of fusions are commonly referred to as phase change materials (PCM).

PCM based TES systems have the potential to help reduce air conditioning requirements because these materials absorb heat at a constant temperature. If a PCM material had a transition temperature just above room temperature, ~30-35 $^{o}$C, the material would absorb heat and prevent the temperature from rising above the transition temperature. These systems consist of two designs. The first design contains the PCM in a bulk container as it melts. This can be accomplished using sealed panels or pouches filled with the PCM [9]. One drawback of this method is that the PCM will escape containment if any leaks develop in the container. Another issue is the additional weight and bulkiness of the containment system. The second PCM system design solves these problems by encapsulating the PCM inside a second solid material. The PCM remains trapped in the solid substrate. A concrete wall with embedded PCM material is an example of this type of system [7]. The major drawback to this method is the challenge of incorporating a large volume fracture of PCM into the substrate without segregation of the PCM and the substrate [10].

## C. PHASE CHANGE MATERIALS

A large variety of phase change material exist with many variations in material properties. PCMs can be subdivided into categories based on the composition of the material. The two main categories of PCMs are organics and inorganics. Organic PCMs can be further divided between paraffin and non-paraffin materials. Inorganic PCMs are divided into salt hydrates and salts. Figure 4 displays the general range of latent heat of fusion and melting temperature for each PCM subcategory.

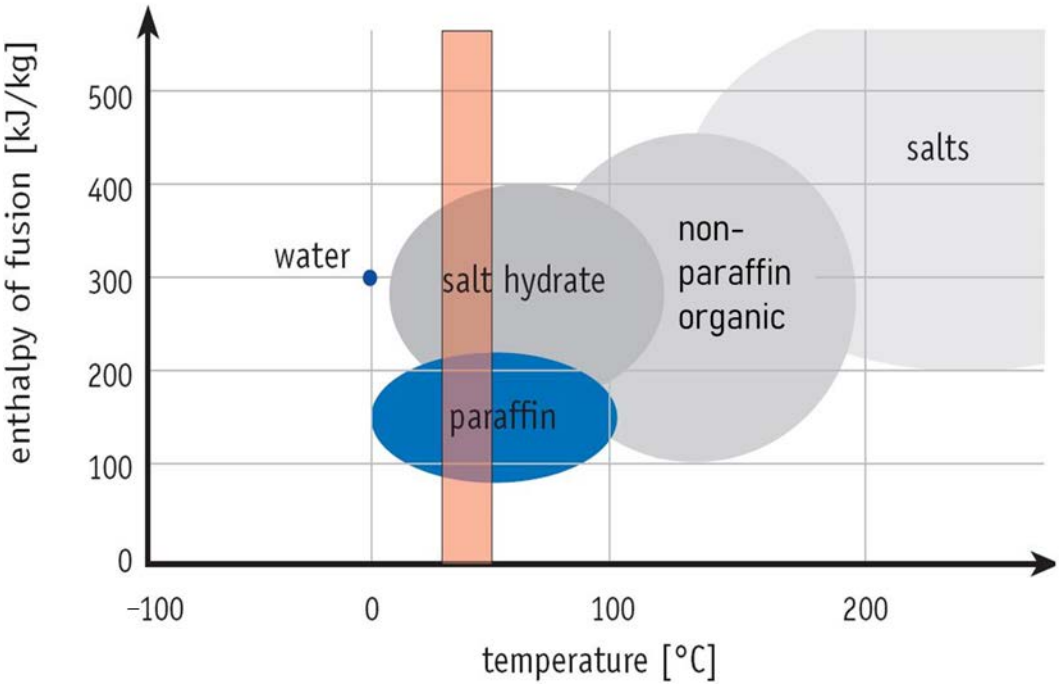


Figure 4. Heat of fusion and temperature range for various PCMs.
Source: [11].

Figure 4 also highlights the range of temperatures from ~25-50 $^{o}$C in red representing temperatures at and above room temperature. Paraffin PCMs consist of a range of different hydrocarbons with varying properties. Generally, the melting point of the paraffin increases as the length of the carbon change increases [7]. This range of temperatures allows for some paraffins to exist in the interested temperature range. The most significant disadvantages of paraffins are low thermal conductivity and moderate flammability [7].

Non-paraffin organics are the largest and most varied category. This group of materials contains several esters, fatty acids, alcohols, and glycols. The large number of materials gives this subcategory a large range of material properties, but few have melting temperatures in the required temperature range. Materials that perform in the required temperature range are generally 2–2.5 times more expensive than paraffin materials and tend to be mildly corrosive [7].

Between the two subcategories of inorganic PCMs, only salt hydrates exist with a transition temperature in the desired temperature range. Salt hydrates typically have a desirably high enthalpy of fusion per unit volume [10]. These materials consist of a mixture of inorganic salts and water. The solid to liquid transformation relies on the splitting of the salt and the water, which results in the separation of the two phases [7]. This causes the solid phase to sink to the bottom of the container and become unavailable to recombine with the water during the reverse cycle.

Paraffin PCM materials were selected as the most suitable to the application of this project. Paraffins exist in the required temperature range with high values of enthalpy of fusion. These materials remain stable in both the solid and liquid phases, allowing for many repeat cycles. The other potential candidate, salt hydrates, has a more complicated melting and solidification reaction which is not always reversible and would make encapsulation of the material more difficult. Including thermal additives in paraffin PCM based TES systems can help the overall thermal properties of the system. Epoxy resins were selected for the current study as the matrix that will contain the paraffin of choice, allowing for the PCM-epoxy system to be cured in various complex shapes and sizes

## D. THERMAL ADDITIVES

The low thermal conductivity of paraffins has been addressed through the inclusion of thermal additives to create paraffin-composite materials. Various studies into different thermally conductive materials have been completed. Metallic materials such as aluminum [12] and copper [13] have been added as micro-sized powders. Metal additives have been shown to increase thermal conductivity, but they also add a significant amount of weight and cost [14]. The large increase in weight associated with metallic additives would reduce the mobility and usefulness of the PCM system. For this reason, only lower weight thermal additives were considered.

Many allotropes of carbon exhibit high thermal conductivity and low densities. Carbon nanofibers (CNFs) and carbon nanotubes (CNTs) are specifically attractive thermal additives due to their high aspect ratios. Both materials have long lengths compared to their small diameters. The major difference between the two is that fibers tend to have less

crystalline structures and are completely filled, while nanotubes have a cylindrical structure with hollow cores and in general higher levels of crystallinity. Commercial CNFs tend to have larger diameters than CNTs [15]. CNFs have been shown to increase the transient response of PCM-CNF mixtures of a soy wax PCM [16]. The thermal conductivity of paraffin wax has been shown to rise with increasing loadings of CNTs [17]. The use of both CNFs and CNTs as thermal additives will be further studied in this project. A large amount of electrically conductive material such as CNFs or CNTs in the PCM-epoxy system will have the advantage to act as electromagnetic shielding and conductor when needed.

Another useful thermal additive is boron nitride (BN). BN has a hexagonal structure analogous to graphite with alternating B and N atoms instead of C atoms. Unlike graphite and other carbon allotropes, BN has a high thermal conductivity without a high electrical conductivity [18]. PCM-epoxy systems containing BN instead of carbon could provide enhanced thermal conductivity without interfering with electrical equipment or blocking electromagnetic signals. A potentially more useful structural form of BN is boron nitride nanotubes (BNNTs) [19]. Both BN and BNNTs were used as thermal additives in this project.

## E. OBJECTIVES AND CHAPTER OUTLINE

The objectives of this project are outlined below. The ultimate goal of the project was to create a PCM-epoxy composite-fabric system applicable for use as a portable and reusable latent heat of fusion TES system.

- Identify a suitable paraffin PCM with melting point ~ 30–40 $^{o}$C, high latent heat of fusion, and high cyclability.
- Develop the formulation and manufacturing technique required to achieve a homogenous encapsulation of PCM in epoxy at a high loading, 40 wt% PCM.
- Determine the effects of thermal additives on the thermal properties of the PCM-epoxy system.

- Identify the PCM-epoxy-additive formulation which best meets the requirements of the project.
- Develop and demonstrate the ability to create a fabric with embedded PCM-epoxy system.

The chapters below are written to explain the process used to achieve the objectives of the project. An overview of the chapters is shown in Figure 5.

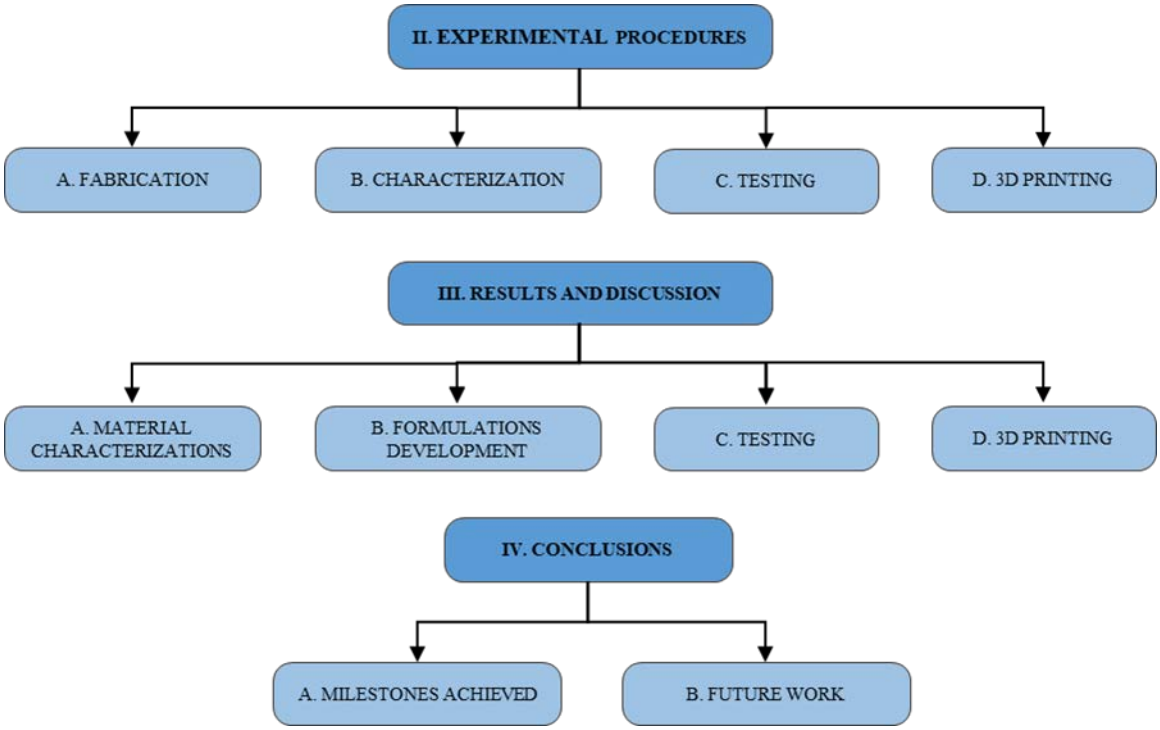


Figure 5. Chapter overview.

As indicated in Figure 5, this study was divided into three main sections. Chapter II provides information on the precursor materials, fabrication methods, and experimental characterization techniques. Chapter III explains the results of the completed work and discusses the implications of these results. Chapter IV concludes the major findings of the research and provides insights on potential future work.

# II. EXPERIMENTAL PROCEDURES

## A. FABRICATION

Two hydrocarbons were selected as potentially possessing the required thermal properties to act as phase change materials (PCM); n-Nonadecane, $CH_3(CH_2)_{17}CH_3$ (Sigma-Aldrich) and n-Eicosane, $CH_3(CH_2)_{18}CH_3$ (Sigma-Aldrich) based on data from Sigma-Aldrich. Nonadecane consists of a straight chain of 19 carbon atoms and has a reported melting point between 30–34 $^oC$. Eicosane is a straight chain of 20 carbon atoms and has a reported melting point between 36–38 $^oC$. The properties of both substances are listed in Table 1.

Table 1. Physical properties of Nonadecane and Eicosane.

| | Nonadecane [7],[20] | Eicosane [7],[21] |
|---|---|---|
| Melting point | 31 - 34 °C | 36 - 38 °C |
| Boiling point | 329 - 331 °C | 343.1°C |
| Density | 0.79 g/cm$^3$ (20 °C) | 0.8 g/cm$^3$ (20 °C) |
| Flash point | >100 °C | > 113 °C |
| Heat of fusion | 244 kJ/kg | 222 kJ/kg |

Adapted from [7], [20], [21].

The epoxy used for each formulation was Epofix (Struers Inc. Cleveland, OH, US). Epofix was selected as the epoxy because it has low viscosity and linear shrinkage. This epoxy consists of two-phases, resin and curing agent, which are mixed together to begin the curing process. The resin consists of Bisphenol-A-Diglycidylether, and the curing agent is Triethylenetetramine. The two components were mixed in a ratio of seven parts resin to one-part curing agent by weight. The mixed epoxy has a viscosity of 550 cP (at 20 $^oC$) and 150 cP (at 50 $^oC$) and requires 8 hours to fully cure [22].

Carbopol 940 (Acros Organics, ThermoFisher Scientific) was selected as a thickening agent to aid with dispersion of the PCM and other additives in the epoxy matrix. Carbopol is commonly used as an additive in commercial gels and creams [23]. Carbopol

is a cross linked polyacrylic acid polymer which aids in suspending powder and improving emulsion stability.

The boron nitride (BN) (Sigma Aldrich [24]) was a white ceramic material. The BN used was a micro-sized powder with particle sizes approximately 1 μm. The shape of the particles was not reported. The boron nitride nanotubes (BNNTs) (BNNT LLC Newport News, Virginia, US) were delivered in a large bundle of interwoven nanotubes. The carbon nanofibers (CNFs) (Sigma Aldrich [25]) were a black powder. The CNFs were reported as graphitized conical platelets with diameter of 100nm and length of 20–200 μm. The carbon nanotubes (CNTs) (Sigma Aldrich [26]) were reported as multi-walled, with an outer diameter of 6–9 nm and length of 5 μm.

The goal of the mixing process was to develop a technique to achieve a fully homogenous mixture. The main tool used in the mixing process was the FlackTek SpeedMixer DAC 150.1 high speed mixer, shown in Figure 6.

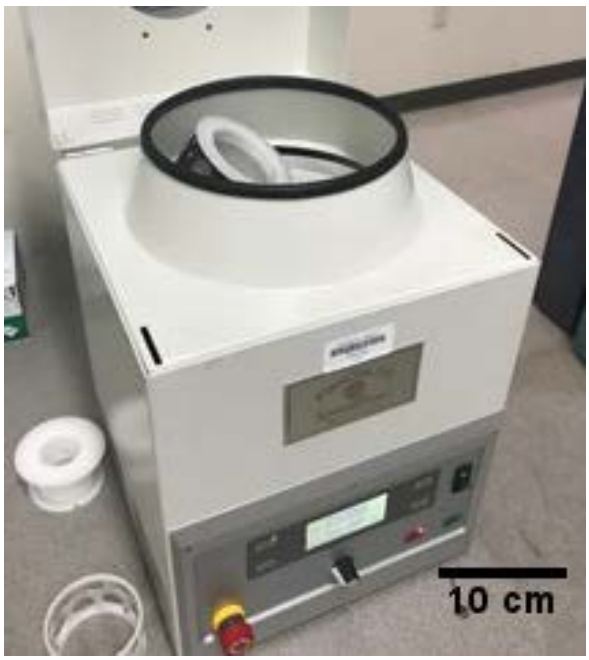


Figure 6. FlackTek SpeedMixer DAC 150.1.

The high-speed mixer was capable of mixing specimen containers at a speed from 1200 rpm to 3500 rpm. Specimen containers varied in size depending on the amount of a formulation being prepared. Most of the formulations were prepared in 6 g batches using a 10 ml container. Some larger batches were prepared using 50 ml containers.

The composition of the Epoxy-PCM formulation and the process by which it was fabricated went through many iterations. Initially, the PCM was broken down mechanically into small solid pieces which could then be mixed into the epoxy resin. It was assumed that the pieces would melt into the resin due to the heat generated during mixing. The PCM is a weak paraffin wax, so mechanically breaking it down into small pieces was not difficult. The difficulty was found while attempting to completely melt the PCM. Due to the PCMs high latent heat of fusion, the pieces remained solid even after repeated cycles of mixing at 3,000 rpm for one minute. This approach was determined to be unfeasible, and the decision was made to preheat the PCM until melted before mixing it into the resin.

The process began by adding the resin and carbopol to the mixing container. These ingredients were then combined at a speed of 3,000 rpm for one minute. The thermally conductive additive was then added, and the mixture was again mixed at a speed of 3,000 rpm for one minute. In a separate container, the PCM was heated and allowed to fully melt. The liquid PCM was added to the mixture at a temperature of about 40 $^{o}$C.

The objective of this step was to end with solid PCM homogenously dispersed and encapsulated by the epoxy. The formulation underwent an initial mixing cycle at a speed of 3,000 for one minute. After this first cycle, the PCM would solidify on the cool walls and roof of the mixing container. Hand mixing using a small metal spatula was required to scrape and mix the solid PCM back into the still warm mixture. Once all solid PCM had melted back into the mixture, the container underwent another mixing cycle. Two or three of these cycles were required for the container to warm enough that PCM solidification on the wall no longer occurred. This thermal equilibrium took longer to occur for larger batches, requiring additional mixing cycles. Once thermal equilibrium was achieved, additional cycles were required until the PCM had dispersed well enough into the mixture that no liquid PCM could be seen separated and floating on top of the rest of the mixture. At this point, the formulation was still warm and at a constant temperature due to the high

latent heat of fusion of the PCM as it solidifies. The solidification of the PCM was accelerated by submerging the bottom of the mixing container in a bath of cool water while mixing by hand with a spatula. After about 15 seconds of cooling, the container underwent a mixing cycle. The formulation was then again submerged in water and allowed to cool down to room temperature while being mixed by hand.

The final ingredient to be added was the liquid curing agent. The container was then given one more mixing cycle at 3,000 rpm for one minute. The curing reaction began with the addition of the curing agent. The completed formulation was then poured into silicon molds to cure or transferred to an extrusion syringe for 3D printing.

## B. CHARACTERIZATION

Differential scanning calorimetry (DSC) was conducted on various samples using a NETZSCH STA 449 F3 Jupiter. A small amount of each sample, about 15–20 mg, was placed in a ceramic test crucible. This crucible was placed into the DSC along with an identical empty test crucible. The two crucibles were heated and cooled by the DSC while the amount of heat required to heat the temperature of the crucibles was measured. Samples were heated from 25 $^{o}$C to 50 $^{o}$C at 1 $^{o}$C/min and then cooled back to 25 $^{o}$C at 1 $^{o}$C/min. This cycle was preformed three times for each sample. The experiments were conducted using a simulated air atmosphere consisting of 20ml/min of oxygen and 80 ml/min of nitrogen. A quartz microbalance within the DSC also recorded a thermogravimetric analysis (TGA) for each sample. The TGA measured any weight changes as the samples underwent the temperature cycles. Post processing of the resulting DSC heat flow vs temperature diagrams allowed for latent heat of fusions to be calculated by integrating the curves which resulted from phase changes occurring in the samples. Data from the DSC experiments was also used to generate enthalpy vs temperature curves for each sample.

Scanning electron microscopy (SEM) imaging was conducted to determine the particle size of the BN powder, CNF and CNTs. A thin layer of each powder was placed onto conductive carbon tape attached to an aluminum stub. Because BN is not electrically conductive, the sample was required to be sputtered with Pt/Pd to create an electrically conductive surface coating. A Cressington Sputter Coater was used to deposit a thin layer

of platinum/palladium. The BN was placed in a vacuum chamber with a low-pressure argon atmosphere. A plate of Pt/Pd was placed above the sample, and a 200 V difference between the Pt/Pd and sample crated a plasma which deposited the Pt/Pd onto the sample. A quartz micro balance was used to measure the weight of deposited metal and estimate the thickness of the coating. A 4 nm layer was deposited on the BN sample. SEM images were taken using secondary electrons from a 20 keV beam with a working distance of 5 mm.

X-Ray diffraction (XRD) was used to determine the crystalline structure of the BN powder. A sample of the BN was placed on a single crystal silicon sample container. The sample was subjected to Cu K-alpha X-rays produced with 40 keV and 15 mA. The XRD ran through a 2 theta range from 10 - 95 degrees, with a step size of 0.02 and a scan speed of 5 degree per minute.

## C. TESTING

A demonstration of the effectiveness of the PCM formulations was conducted using a heated sand bath. The purpose of this experiment was not to collect further data on the thermal properties of the formulations, but rather to provide a practical demonstration of the effectiveness of the formulations. Each sample consisted of a six-gram disk with a diameter of 30mm. The experimental setup is shown in Figure 7.

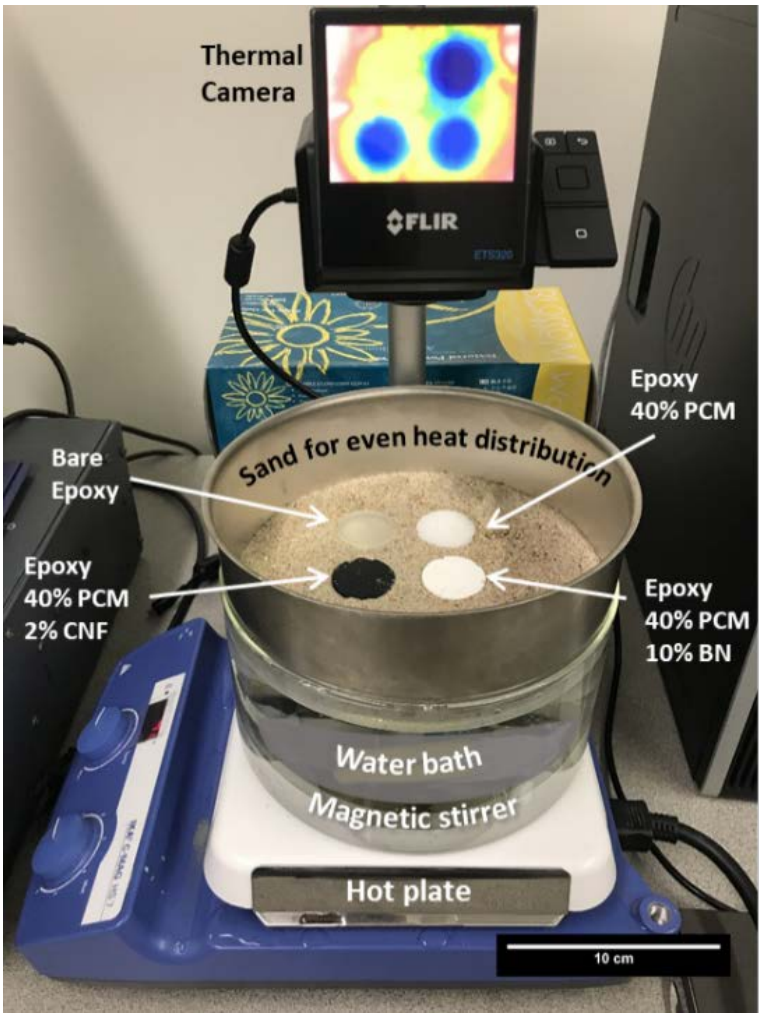


Figure 7. Experimental setup of sand bath demonstration.

A 3 cm layer of sand was sifted into a large metal bowl. This bowl was then placed onto of a glass container of water, with water level touching the underside of the metal bowl. The water sat on a hot plate set to 90 $^{o}$C with a magnetic stirrer continuously mixing the water at a slow speed. Although the hot plate was set to 90 $^{o}$C, the actual temperature of the water was not measured during the experiment. A FLIR ES320 downward facing infrared camera was used to measure the surface temperature of the sand and samples.

The experiment began by allowing the sand to come to thermal equilibrium and achieve an even heat distribution across its surface. The sand was mixed as it was heated, and the system reached a satisfactory equilibrium after approximately 30 minutes, with a surface temperature of 35 $^{o}$C. The four samples were placed in the sand simultaneously,

and each was pressed into the sand so that the top surface of the samples was even with the surface of the sand. The infrared camera was used to record an average surface temperature for each of the samples as well as an average sand temperature calculated using multiple points in the sand. The samples were warmed by the sand until they reached thermal equilibrium with the environment. The experiment concluded 55 minutes after the samples were placed into the sand.

Thermal conductivity tests were performed on selected formulations by Thermal Analysis Labs Ltd (TAL) located at Fredericton, N.B. Canada. Formulations were prepared and molded into cylinders 2 cm thick with a diameter of 3 cm at NPS laboratories following the procedure previously described. The top and bottom surfaces of the Epoxy-PCM-xxx cylinders were polished with SiC grind paper 2400 to provide an even contact surface. The completed formulations were shipped to TAL for the testing. Figure 8 shows the setup used for the thermal conductivity and thermal effusivity measurements.

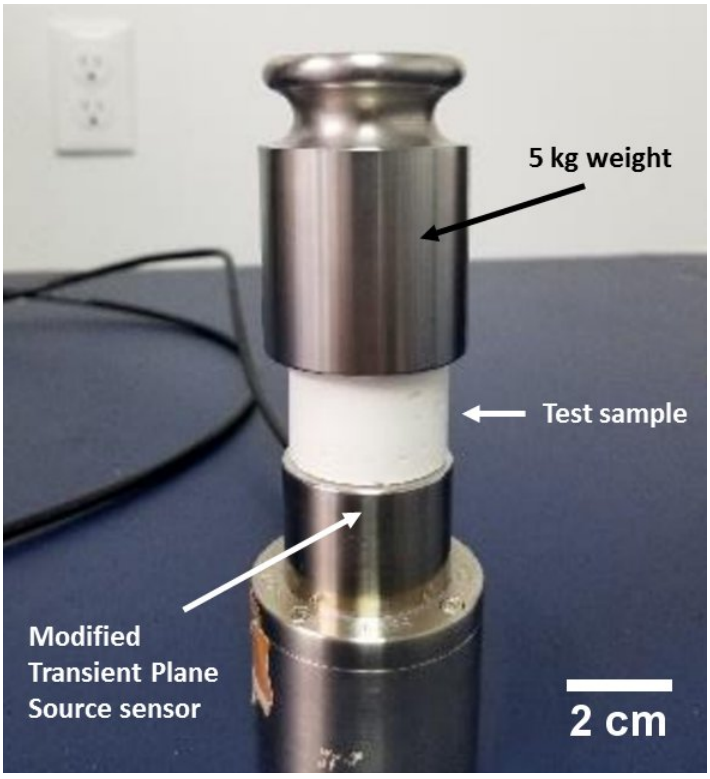


Figure 8. TAL experimental setup.

The sample was placed on top of a Modified Transient Plane Source sensor, and a 5 kg weight placed on top of the sample ensured solid thermal contact. The sensor heated the underside of the sample by approximately 1 – 3 $^{o}$C using a known amount of heat. The dissipation of this heat away from the sensor interface is measured by monitoring the voltage at the sensor interface. The thermal conductivity and effusivity of the sample could then be calculated in compliance with ASTM Standard D7984-16.

## D. 3D PRINTING

Work was done to integrate the final PCM formulation onto a fabric. A SE3D R3bel mini gel 3D printer was used to extrude the formulation. The 3D printing setup is shown in Figure 9.


Figure 9. SE3D Rebel mini gel 3D printer setup.

The formulation was placed into the extruding syringe, and a section of fabric was secured to the printing plate. Two types of fabrics were used for the printing, nylon and Kevlar. These two fabrics represent possible materials which could be used as the base

substrate of the PCM lining system. The Kevlar was yellow and coarsely woven, and the nylon was black and very finely woven.

The computer-controlled nozzle was then used to deposit the PCM formulation at a controllable extrusion width and height, and the resulting shape of the formulation on the fabric could be adjusted. Solidworks was used to create the part file of basic square, circle, and hexagonal shapes. The part files were then converted to g-code using Slic3r. Ponterface software was used to run the printer using the generated g-code.

The printer operated at a print speed of 2 mm/sec. The nozzle had a diameter of 1.5 mm, and the nozzle tip was set 1 mm above the printing surface. For printing of the epoxy only, the nozzle diameter setting was set to 1.25 mm to provide some overlap between two adjacent extruded lines. The extrusion multiplier was set to 0.15 to achieve a continuous even flow.

The settings were different while printing the thicker EC-PCM40 (Epoxy-Carbopol 5 wt%-PCM 40 wt%). The nozzle diameter was increased to 1.4 because the printed lines did not spread as much. The extrusion multiplier was increased to 0.5 in order to achieve a continuous flow. A full print was not completed with this formulation because the pressure of being extruded from the nozzle appeared to cause segregation which caused the nozzle to jam. A larger diameter nozzle would help the problem, and new print settings would need to be found for the larger nozzle.

Molding the PCM formulation onto the fabric was also explored. Using molds allowed for the shaping of PCM formulations which were too viscous to easily extrude. The mold setup is shown in Figure 10.

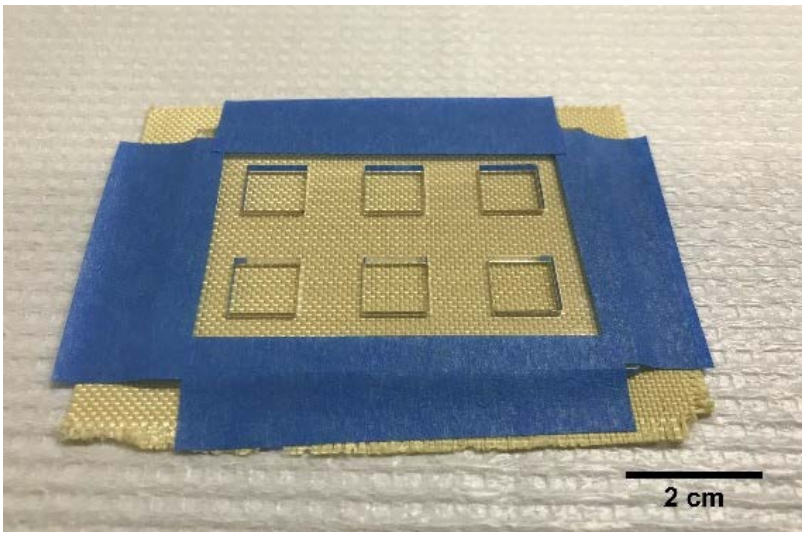


Figure 10. PCM-Epoxy fabric mold.

Six 1 cm by 1 cm squares were cut into a 2 mm thick acrylic sheet using a Spirit GCC LaserPro cutting machine. The resulting mold was then taped down to the fabric. The mold was filled with newly mixed material and allowed to cure overnight. Once cured, the mold could be removed by holding down the solid sections of the PCM formulation while peeling away the acrylic mold.

# III. RESULTS AND DISCUSSION

## A. MATERIAL CHARACTERIZATIONS

The two PCMs were evaluated to determine which should be used in the formulation. The melting point and the latent heat of fusion were the major considerations for the selection of the PCM. A small sample of n-Nonadecane and n-Eicosane were placed into the STA for DSC and TGA evaluation. Figure 11 shows the results of the DSC.

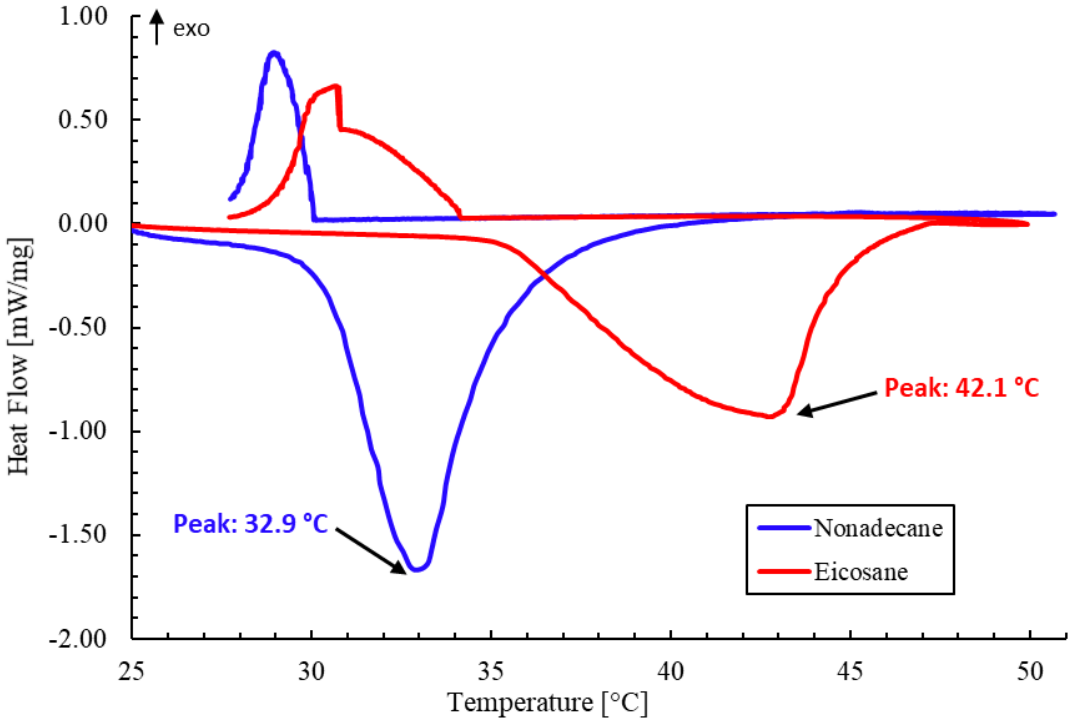


Figure 11. DSC results for n-Nonadecane and n-Eicosane.

The DSC measures the temperature difference between an empty crucible and a crucible with a small amount of the sample. The DSC slowly raises and lowers the temperature of the test chamber. Phase changes occur at a constant temperature, so the temperature of the sample crucible will be constant until the phase change in complete. On an increasing temperature scan, the temperature of the sample crucible remains constant as the temperature of the empty crucible continues to rise. The DSC measures the amount of

heat inputted into the system as the temperature of the sample crucible remains constant. This input of energy is shown as the downward facing endothermic peaks in Fig 10. The curves indicate the amount of additional heat inputted into the system as the temperature was increased. The latent heat of fusion for the solid to liquid transition is found by calculating the area under this curve. The opposite process occurs as the DSC decreases the test chamber temperature. The sample crucible will release heat as it solidifies, producing an exothermic peak.

The DSC results show that n-Nonadecane has a lower melting temperature and a narrower peak for the solid to liquid transition. The melting temperature of n-Nonadecane was found to be 32.9 $^{o}$C, and the latent heat of fusion was calculated as 160.2 J/g. The melting temperature of n-Eicosane was found to be 42.1 $^{o}$C, and the latent heat of fusion was calculated as 179.8 J/g. The melting temperature of n-Eicosane was found to be too high above room temperature to be useful. Eicosane has a higher latent heat of fusion, but the latent heat of fusion of n-Nonadecane is still high enough to be a useful PCM material. Nonadecane was selected as the PCM to be used in the Epoxy-PCM formulations.

The SEM was used to determine the size and structure of each thermal additive. Figure 12 shows a side by side comparison at an identical scale of the BN micropowder and the BNNT.

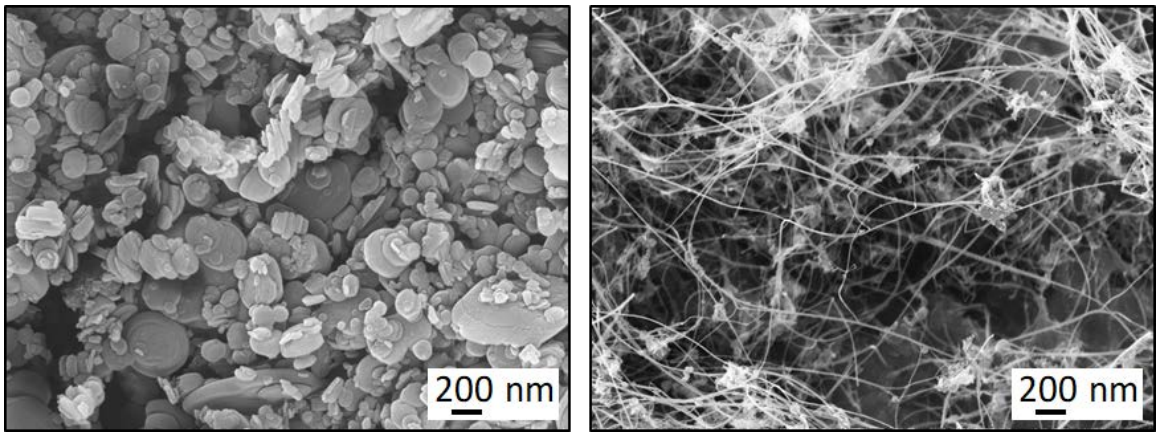


Figure 12. SEM images of BN micropowder (left) and BN nanotubes (right).

The particles of the BN micropowder appeared to have a platelet like structure with a wide range of diameters. The diameters of the particles ranged from 40–530 nm, with an average size of ~150 nm. The BNNT was found to have a web like filament structure. The diameter ranged from 6–24 nm. The nanotubes appeared to be clumped together in some areas and spread out in others. Figure 13 shows the comparison between the carbon containing thermal additives.

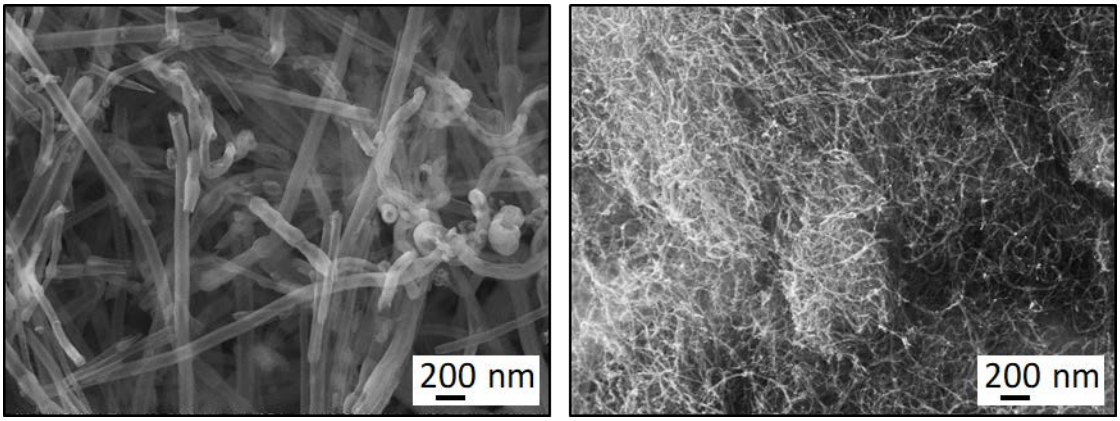


Figure 13. SEM images of carbon nanofibers (left), and carbon nanotubes (right).

The size differences between the micro and nano scale carbon additives were similar to the BN additives. The CNF were found to have an average diameter of ~ 150 nm. The fibers were evenly spaced throughout without large clumps. The CNT consisted of bundles of very fine nanotube structures. The CNT had diameters of only 4–15 nm.

XRD of the BN micropowder revealed the expected crystalline structure. The diffraction spectra of the XRD experiment is shown in Figure 14.

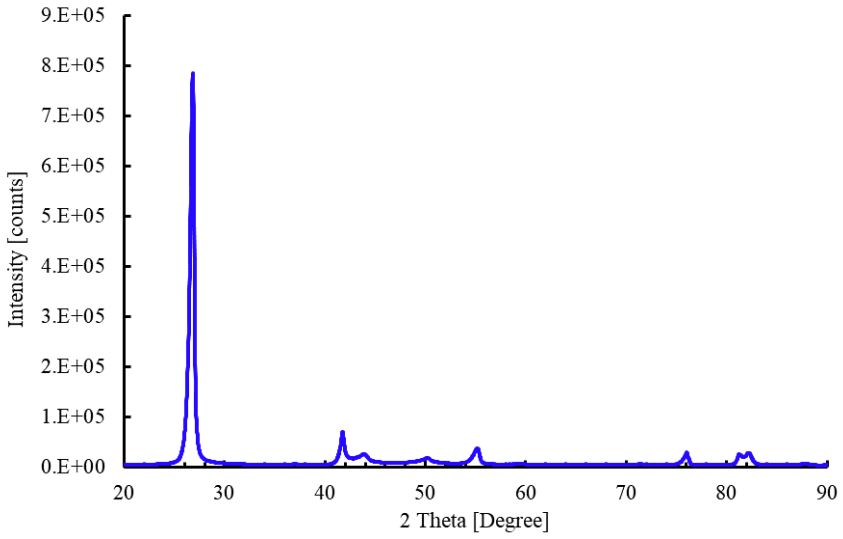


Figure 14. XRD counts for BN micropowder.

The sharp peaks indicate a highly crystalline structure which diffracts x-rays at specific angles. The spectra matched a known spectrum from the XRD database. The BN was found to have a hexagonal crystalline structure. Figure 15 shows the information associated with a BN crystal.

| PDF Card No.: 04-014-3363 Quality:I | | | | | | |
|---|---|---|---|---|---|---|
| Sub-File Name: | Inorganic, Alloy&Metal, LPF Pattern | | | | | |
| Formula: | B N | | | | | |
| Name: | Boron Nitride | | | | | I/Ic (RIR)= 2.06 |
| Crystal System: | Hexagonal | Space Group: | P-6m2(187) | Dmeas: | | |
| Cell Parameters: | a= 2.4982 | b= | 2.4982 | c= | 6.6357 | |
| | Alpha= 90.000 | Beta= | 90.000 | Gamma= | 120.000 | |
| | Volume= 35.866 | Z= | 2 | | | |
| Reference: | Kurakevych O.O., Solozhenko V.L. Acta Crystallogr., Sec. | | | | | |

Figure 15. Boron Nitride crystalline information.

## B. FORMULATION DEVELOPMENT

The composition of the PCM epoxy system and the fabrication process underwent multiple iterations as the project developed. First, a base formulation was developed to achieve a homogenous encapsulation of PCM in the epoxy. Once a base formulation was created, thermal additives were included. The thermal properties of these formulations were found to identify the effects of the thermal additives. A final formulation was selected which best met the requirements of the PCM epoxy system.

### 1. Base Formulation Development

Experiments were conducted attempting to combine liquid PCM with the epoxy resin. Two formulations were attempted, one to combine 30wt% PCM and one to combine 40wt% PCM. The liquid PCM and epoxy resin were mixed at 3,000 rpm for two minutes, and then mixed at 3,500 rpm for three minutes. The curing agent was added and mixed in by hand. The formulation was then poured into silicon molds to cure. Figure 16 shows the fully cured Epxoy-PCM40 formulation.

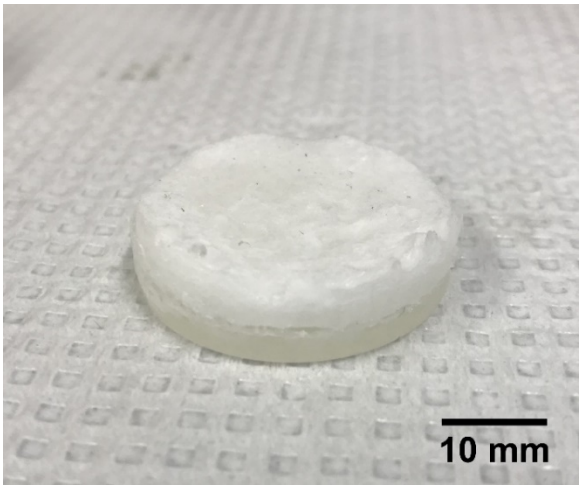


Figure 16. Epoxy-PCM40 highly segregated.

The two liquid phases completed segregated over time as the formulation cured. The PCM rose and formed the top white layer. The epoxy solidified underneath, and it is visible as the slightly darker layer. The segregation was less extreme for the formulation

with only 30wt% PCM, but a similar two-layer segregation could be seen. This experiment clearly demonstrated the need for an additive to help emulsify the formulation.

Carbopol was included into the next fabrication attempt. This formulation consisted of the epoxy with 40wt% PCM and 5wt% carbopol. The mixing followed the same procure as previously described. First the carbopol was combined into the epoxy resin, and then the liquid PCM was added. The mixture was thoroughly combined until homogenous, then then the curing agent was added. Figure 17 shows the cured formulation.

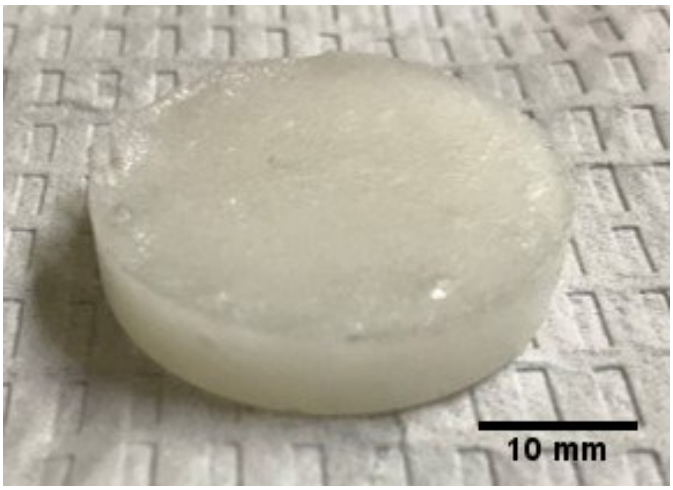


Figure 17. EC-PCM40 homogenous mixture.

The inclusion of carbopol greatly increased the ability of the liquid PCM and epoxy resin to combine. The two liquids did not segregate apart as the formulation cured, and the PCM remained encapsulated by the epoxy. Now that a stable formulation was found, the effects of including thermal additives could be explored. The inclusion of thermal additives into the formulations did not change the overall fabrication process. The thermal additives were mixed into the epoxy resin with the Carbopol before the liquid PCM was added.

The DSC was then used to evaluate the combination of homogenously combined mixture of the epoxy, carbopol, and PCM. A sample of pure epoxy and a sample of EC-PCM40 were tested, and Figure 18 shows a comparison of these tests with the pure PCM.

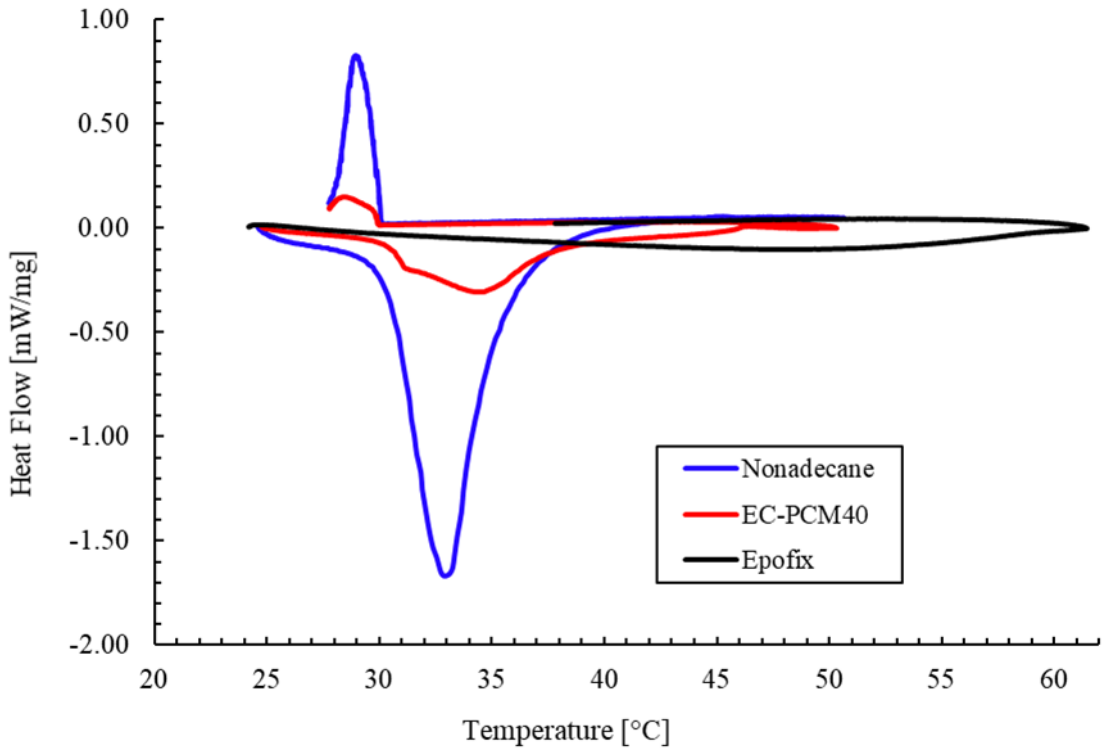


Figure 18. Epoxy-PCM mixture comparison.

The pure epoxy did not show any heat flow signal. This result was expected because no phase transformations should be occurring in the epoxy at this temperature range. The heat flow signal for the EC-PCM40 also showed the expected result. The PCM within the epoxy underwent the same phase transformation as the pure PCM, except that the transformation produced a less pronounced and more spread out peak. The amount of heat absorbed was 27.2 J/g, which is 17% of the pure PCMs latent heat of fusion of 160.2 J/g.

### 2. Formulations Containing BN

DSC testing was completed for each of the formulations containing BN thermal additives. The results of the DSC testing are shown in Figure 19, and the latent heat of fusion for each formulation is summarized in Table 2.

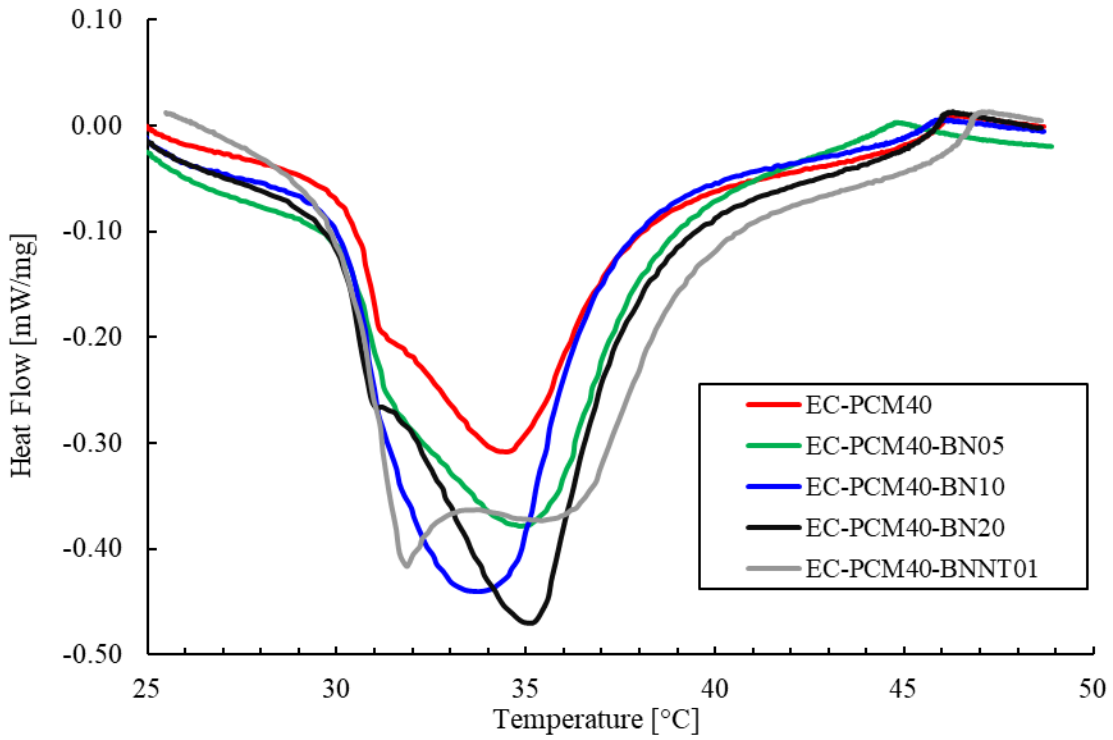


Figure 19. DSC results for BN and BNNT additives.

Table 2. Thermal results for BN containing formulations.

| Formulation | Latent Heat [J/g] | % of Nonadecane | EC-PCM40 Improvement [J/g] | Peak Temp. [°C] |
|---|---|---|---|---|
| Nonadecane | 160.2 | - | - | 32.9 |
| EC-PCM40 | 27.2 | 17.0 | - | 34.4 |
| EC-PCM40-BN05 | 32.2 | 20.1 | + 5.0 | 34.8 |
| EC-PCM40-BN10 | 41.6 | 26.0 | + 14.4 | 33.7 |
| EC-PCM40-BN20 | 42.6 | 26.6 | + 15.4 | 35.1 |
| EC-PCM40-BNNT01 | 59.5 | 37.1 | + 32.3 | 35.5 |

BN micropowder showed a promising increase in the heat flow signal of the system. 5 wt % increased the latent heat by 5.0 J/g, and 10 wt% increased it by 14.4 J/g. The addition of more BN past 10 wt% did not produce a significant increase, with 20 wt% giving an increase of 15.4 J/g. The largest increases in latent heat was produced though the

use of the nano scale thermal additive. The addition of 1 wt% BNNTs increased latent heat by 32.3 J/g.

The mechanical effects of the additives were observed qualitatively throughout the fabrication process. The most notable change was an increase in viscosity with an increase in thermal additive loading. The best results were found by using 10 wt% BN. This formulation gave an increase in latent heat of fusion and did not overly increase the viscosity. The 20 wt% BN was deemed to be too viscous, acting more as a solid paste. The BNNT formulation appeared to have poor mechanical robustness once cured. It was softer than the BN formulations, and it was able to be easily bent and broken apart by hand.

### 3. Formulations Containing Carbon

DSC testing was completed for each of the formulations containing BN thermal additives. The results of the DSC testing are shown in Figure 20, and the latent heat of fusion for each formulation is summarized in Table 3.

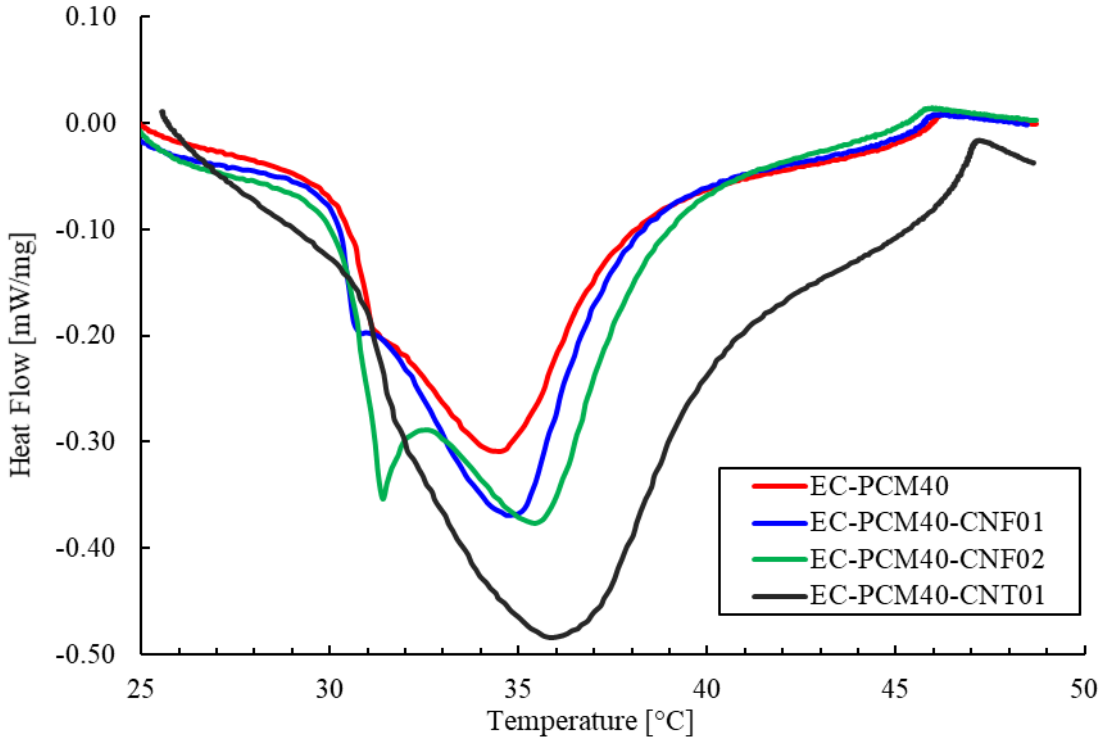


Figure 20. DSC results for CNF and CNT additives.

Table 3. Thermal results for carbon containing formulations.

| Formulation | Latent Heat [J/g] | % of Nonadecane | EC-PCM40 Improvement [J/g] | Peak Temp. [$^{o}$C] |
|---|---|---|---|---|
| Nonadecane | 160.2 | - | - | 32.9 |
| EC-PCM40 | 27.2 | 17.0 | - | 34.4 |
| EC-PCM40-CNF01 | 27.1 | 16.9 | - 0.1 | 34.6 |
| EC-PCM40-CNF02 | 39.6 | 24.7 | + 12.4 | 35.4 |
| EC-PCM40-CNT01 | 74.6 | 46.6 | + 47.4 | 35.8 |

The improvements gained by the addition of CNFs were modest. No change was found with 1 wt%, and a 12.4 J/g improvement was gained with 2 wt%. The largest increase in latent heat was again produced though the use of the nano scale thermal additive. The addition of 1 wt% CNTs increased latent heat by 47.4 J/g, and it had a value 46.6% of the pure PCM. This result was the largest increase to the latent heat of fusion of the PCM system. The use of the carbon nanofibers and nanotubes had a large increase in the viscosity of the mixture. This large increase in viscosity is most likely due to the large aspect ratio of the carbon additives. The viscosity increase was higher for the CNTs than the CNFs.

## 4. Final Formulation Selection

The EC-PCM40-BN10 was selected as the most promising for use in the PCM fabric TES system. This selection was based both on the favorable performance of the BN and on the negative impacts associated with using the other additives. The 10 wt% BN formulation was selected as the optimum amount due to the increase to thermal performance without too much of an increase in viscosity. The 5 wt% BN did not have a high impact on thermal performance, and the 20 wt% BN had too much of a negative impact on the mechanical properties. The use of the BNNTs was ruled out based on the negative impacts to the mechanical robustness.

The carbon-based thermal additives showed promising thermal properties but were not selected due to problems inherent with carbon based additives. The electrical conductivity of the PCM system may interfere with electromagnetic signals passing

through the material. This interference may restrict the applications in which the fabric lining could be used. The black color of the carbon additives is another potential issue. The dark color will absorb more solar radiation and potentially restrict the fabric lining to inside use only. The white color of the BN both reduces the absorption of solar radiation and allows for the formulation to be dyed to a desired final color.

The final issue considered was the cost of each thermal additive. The BN micropowder costs ~$1.8/g [24]. The CNF cost ~$5.4/g [25]. The CNT cost ~$141/g [26]. These costs are highly dependent upon the manufacturing technique used and the quality of the material required, but they show the general spread for the cost of each additive. CNF are not prohibitively more expensive than BN, but the cost associated with using CNT is a major concern.

A final DSC experiment was conducted to demonstrate the cyclability of the PCM epoxy system. The EC-PCM40-BN10 formulation underwent multiple cycles from 25 $^{o}$C to 50 $^{o}$C at 1 $^{o}$C/min. The results of these cycles are shown in Figure 21.

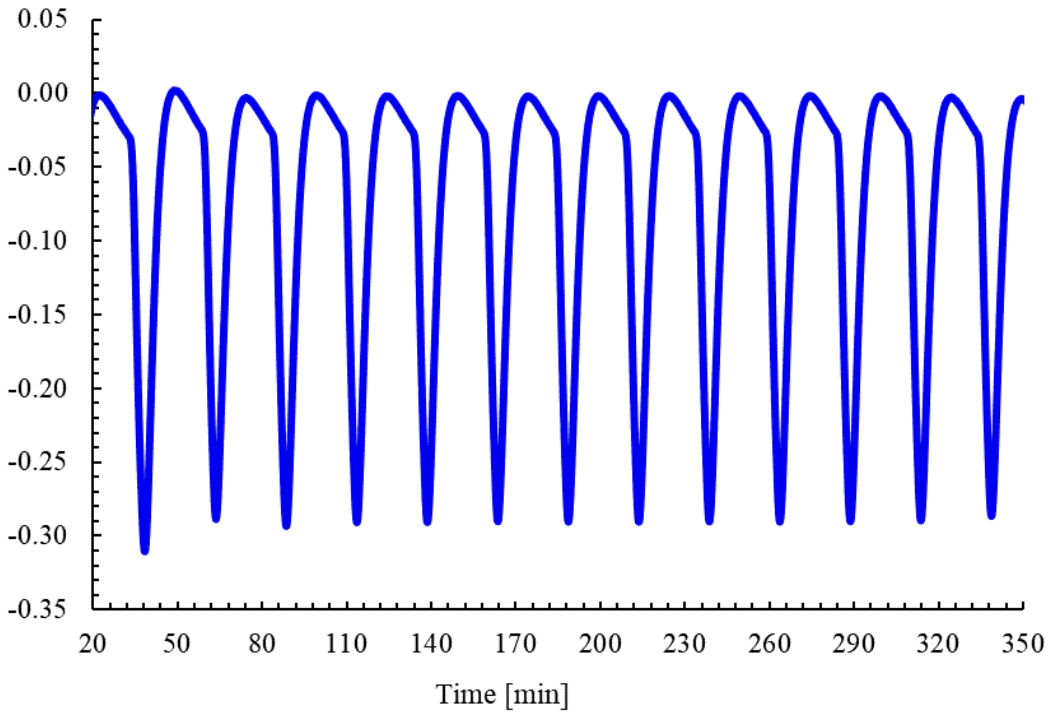


Figure 21. Cyclability results of PCM epoxy system.

The heat flow signal of the formulation does not degrade over time. Each endothermic peak reaches down to the same value during each cycle. This result shows the full reversibility of the paraffin PCM. The high reversibility of this PCM allows it to be suitable for use in a latent heat of fusion TES system.

The thermal properties of the EC-PCM40-BN10 formulation have been shared with the Spanish Naval Academy. Collaborators at that institution are working on an analytical model of the PCM system to determine how much energy will be saved by the use of a liner in a portable setup. This model will be used to estimate the effectiveness of a full-sized system. The model will provide useful insights potential material properties changes which could be researched to improve the effectiveness of the PCM system. The results of this project have also been shared with the Naval Postgraduate School (NPS) Business School for use in a business case study. They are working to determine the monetary benefits of using PCM systems to reduce the military's energy use. Both studies are ongoing, and each will provide useful insights into potential improvements to the PCM system.

## C. TESTING

The sand bath experiment provided a useful proof of concept demonstration of the PCM system. The experiment showed the difference in the thermal performance of the bare epoxy and the PCM system. The performance of different thermal additives was also shown. The thermal camera measured the temperature of the sand and the samples over time as they heated to thermal equilibrium. The results of these measurements are shown in Figure 22.

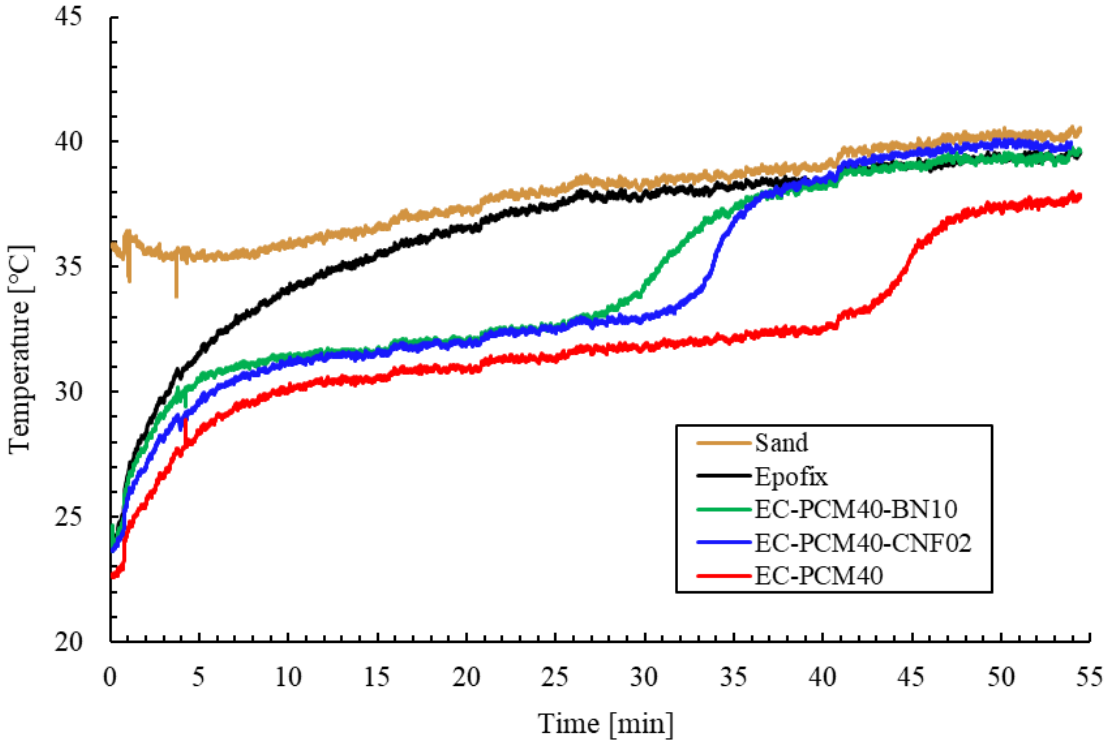


Figure 22. Temperature vs. time for sand bath experiment.

The results of the experiment show the potential advantage of using the PCM system. The sand temperature is shown in gold. The temperature of the sand began at 35 $^{o}$C and raised as heat was inputted into the system. All samples were placed into the sand at room temperature. The temperature of the samples were then increased as they began to reach thermal equilibrium with the surrounding sand. Figure 23 shows infrared images of the samples at the beginning of the experiment, after 15 minutes, and after 35 minutes.

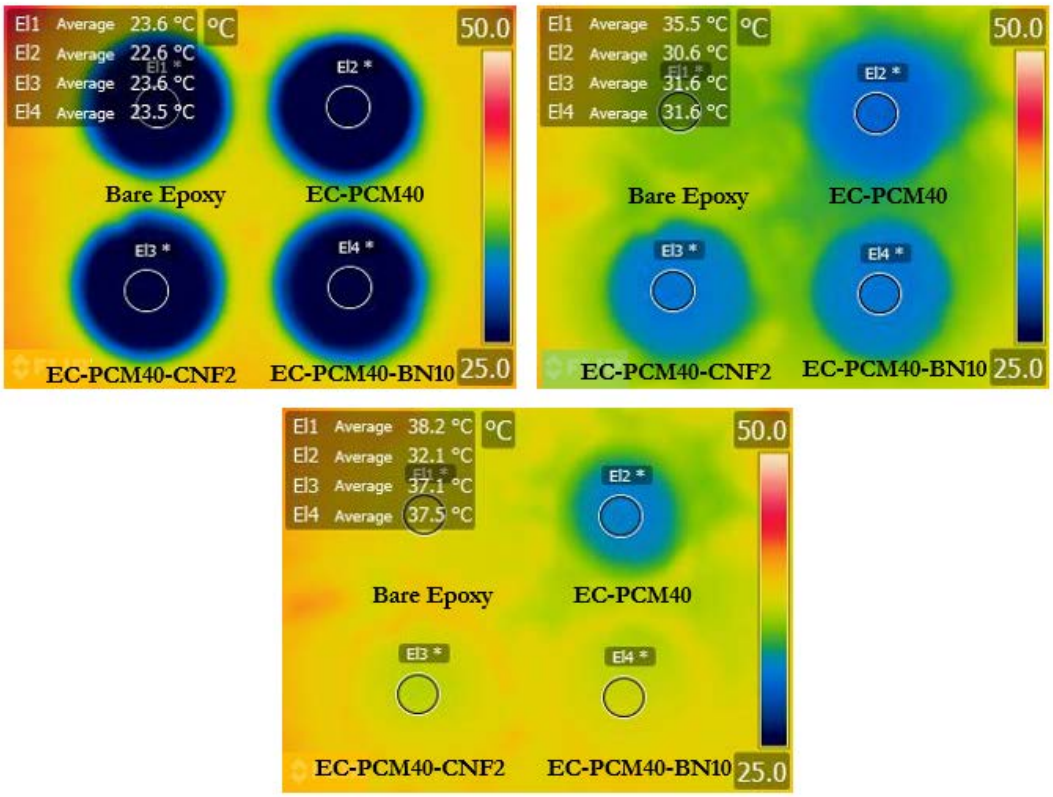


Figure 23. Infrared images of samples, 0 minutes (top left), 15 minutes (top right), 35 minutes (bottom).

The sample of bare epoxy was the first to reach thermal equilibrium. The temperature of the epoxy rose uninterrupted until equaling the temperature of the sand after 15 minutes. The samples which included the PCM behaved as expected. All three demonstrated the pause in temperature raise at 32 ºC associated with the phase change. The PCM formulations absorbed heat from the surrounding sand during this transition and remained at a constant temperature.

The formulations with a higher thermal conductivity remained at the constant temperature for a shorter amount of time. The temperature of the BN10 formulation began to increase at 28 minutes, and the temperature of the CNF02 formulation increased at 32 minutes. The image at 35 minutes shows the two thermally conductive formulations at

thermal equilibrium with the sand. The EC-PCM40 eventually reached thermal equilibrium after 45 minutes.

TAL completed the thermal conductivity and thermal effusivity experiments and delivered a report with the results. Tables 4 and 5 show the values found for thermal conductivity and thermal effusivity as well as the error associated with each measurement.

Table 4. Thermal conductivity results.

| Sample | Temperature(°C) | Result | Test Number | | | Average |
|---|---|---|---|---|---|---|
| | | | 1 | 2 | 3 | |
| **Epoxy** | **RT** | k (W/mK) | 0.270 | 0.276 | 0.280 | **0.275** |
| | | RSD (%) | 0.3 | 0.5 | 0.2 | **1.5** |
| **EC-PCM40** | **RT** | k (W/mK) | 0.295 | 0.292 | 0.294 | **0.293** |
| | | RSD (%) | 0.6 | 0.5 | 0.4 | **0.6** |
| **EC-PCM40-CNF02** | **RT** | k (W/mK) | 0.306 | 0.301 | 0.301 | **0.303** |
| | | RSD (%) | 0.2 | 0.2 | 0.1 | **0.9** |
| **EC-PCM40-BN10** | **RT** | k (W/mK) | 0.413 | 0.416 | 0.417 | **0.415** |
| | | RSD (%) | 0.4 | 0.3 | 0.4 | **0.5** |

Table 5. Thermal effusivity results.

| Sample | Temperature (°C) | Result | Test Number | | | Average |
|---|---|---|---|---|---|---|
| | | | 1 | 2 | 3 | |
| **Epoxy** | **RT** | α (Ws½/m²K) | 611 | 617 | 622 | **617** |
| | | RSD (%) | 0.2 | 0.2 | 0.1 | **0.8** |
| **EC-PCM40** | **RT** | α (Ws½/m²K) | 639 | 636 | 638 | **638** |
| | | RSD (%) | 0.3 | 0.3 | 0.2 | **0.3** |
| **EC-PCM40-CNF02** | **RT** | α (Ws½/m²K) | 653 | 647 | 647 | **649** |
| | | RSD (%) | 0.1 | 0.1 | 0.1 | **0.5** |
| **EC-PCM40-BN10** | **RT** | α (Ws½/m²K) | 772 | 774 | 776 | **774** |
| | | RSD (%) | 0.2 | 0.2 | 0.2 | **0.3** |

All reported values were found with only small variation between tests. An average value was calculated using the multiple tests. The thermal additives successfully increased both the thermal conductivity and effusivity. Because the two properties are similar, the

values for the thermal conductivities and effusivities followed the same trend. The epoxy had lowest values, which was the expected result. The addition of carbopol and PCM slightly increased the values. The increase associated with the addition of 2 wt% CNF was unexpectedly low. The largest increase was given by the addition of 10 wt% BN. The BN increased the thermal conductivity by 41.6 % compared to the formulation without any thermal additives.

## D. 3D PRINTING

The application of the 3D printer to extrude the formulation was first developed using only the epoxy. Epoxy became more viscous with the addition of PCM and thermal additives, so beginning with only epoxy allowed for base line setting for the printer to be determined. The successful epoxy prints are shown in Figure 24.

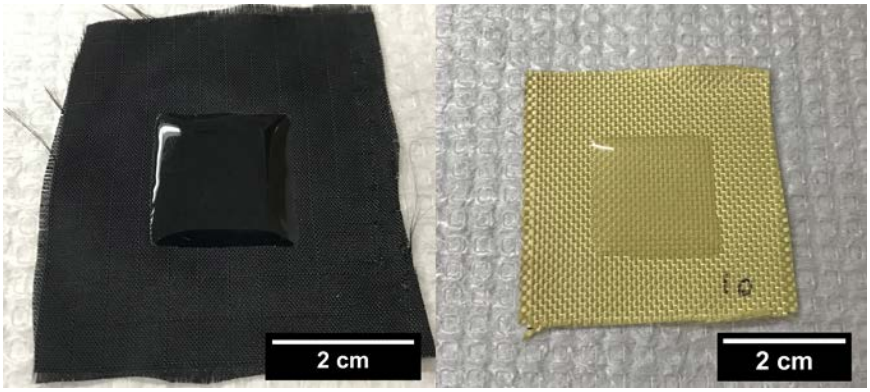


Figure 24. Epoxy extruded onto (left) nylon and (right) Kevlar.

The settings were refined to successfully print an even layer of epoxy in the desired shape. Once cured, the epoxy remained firmly bonded to both the nylon and the Kevlar fabrics. Only a simple demonstration square was printed onto the fabric, but more complicated shapes and patterns of shapes could be designed to give the lining system more flexibility.

Once the epoxy settings were determined, the EC-PCM40 formulation was attempted to be printed. The viscosity of this formulation proved to be a major challenge for the syringe-based 3D printer. A large force was required to push the formulation

through the narrow nozzle. The nozzle also became jammed with material which could not could not be overcome by the force of the printer. These obstructions had to be removed by taking the syringe out of the printer and manually exerting enough force to overcome them. The large amount of force involved with extrusion appeared to cause segregation. The liquid epoxy could more easily extrude from the syringe which left behind more solid carbopol and PCM. This segregation increased the likelihood of jamming and altered the composition of the printed formulation. Figure 25 shows material segregated in the syringe at the end of the printing attempt.


Figure 25. Segregated carbopol and PCM after printing attempt.

A large amount of solid white material remained in the syringe at the end of the printing attempt. Successful printer settings were not found. The attempt shows the need to find a larger diameter nozzle or a larger syringe for this 3D printing setup. Another potential solution could be to reduce the viscosity of the formulation by increasing the extrusion temperature or by including another additive. To demonstrate the fabrication of a fabric liner with the final EC-PCM40-BN10 formulation, a mold was used to create a flexible pattern of PCM material. Figure 26 shows the liner after the mold was removed.

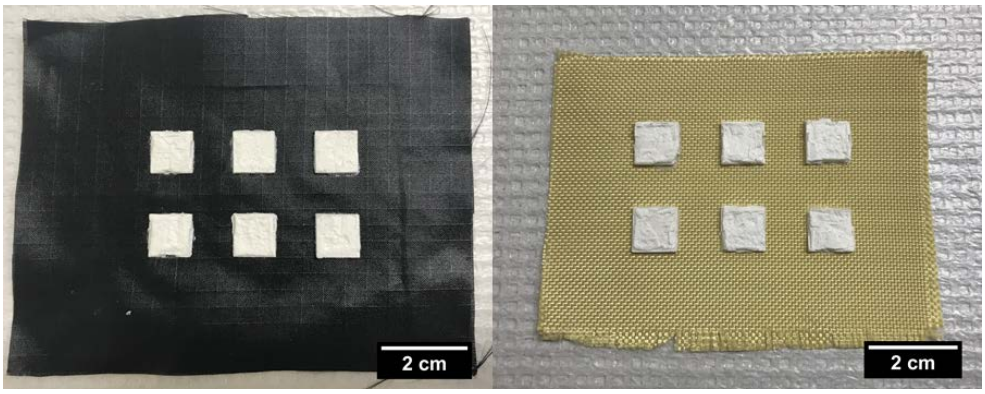


Figure 26. EC-PCM40-BN10 molded onto nylon (left) and Kevlar. (right)

Once cured, the mold was able to be separated by holding down the squares while peeling away the mold. The PCM material became strongly bonded to the fabric material. The square pattern allowed for the liner to fold between the solid selections. Such a flexible system could be scaled up into a larger pattern.

Vibration assisted printing (VAP) helped solve the problem of 3D printing the viscous material. VAP used resonant nozzle vibrations to reduce the effective friction at the nozzle. A vibration amplitude of 8 µm and a back pressure of 25 psig was used to successfully extrude the EC-PCM40-BN10 formulation onto nylon. Figure 27 shows the resulting flexible Epoxy-PCM liner.

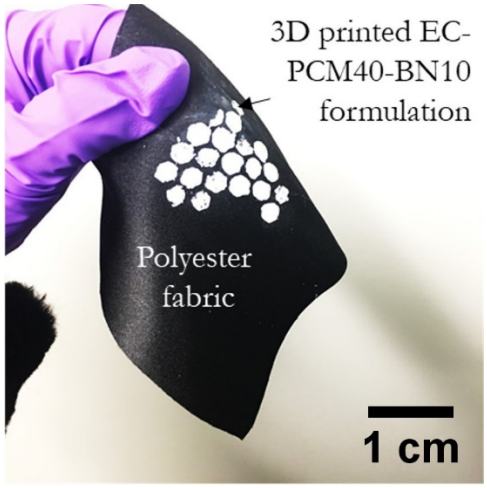


Figure 27. EC-PCM40-BN10 3D-printed with VAP system.

# IV. CONCLUSIONS

## A. MILESTONES ACHIEVED

The goal of the project was to create a PCM fabric system applicable for use as a portable and reusable latent heat of fusion TES system. The milestones achieved during this project have each contributed to this goal. A suitable paraffin PCM was selected, n-Nonadecane, with a melting point within the targeted range, ~32 $^{o}$C, and a high latent heat of fusion, 160.2 J/g. The inclusion of 5 wt% carbopol proved to aid in dispersion, and the fabrication technique developed successfully achieved a homogenous encapsulation of PCM in epoxy at a loading of 40 wt% PCM. The BN and carbon-based thermal additives were characterized through SEM and XRD techniques, and their thermal effects were determined though DSC and thermal conductivity experiments. Through these experiments, the EC-PCM40-BN10 formulation was selected as most meeting the project requirements. This formulation had a high thermal conductivity and heat of fusion, and BN had many beneficial properties including low cost, white color, and low electrical conductivity. The use of the PCM system was demonstrated using a thermal camera, the PCM system was embedded onto both nylon and Kevlar fabric. A simple demonstration of the completed PCM-epoxy fabric liner system was created to demonstrate the final overall structure of the latent heat of fusion TES system.

## B. FUTURE WORK

The mechanical properties of the PCM composite and liner system should also be characterized. This project focused on the thermal properties of the system, but the actual system would be required to remain structurally sound in potentially hazardous environments. The mechanical demands on the system may prove to be significant, which may require modifications to the formulation. The 3d printing onto the fabric requires addition research, and the strength of the bond to the fabric may need to be improved.

The collaboration with the Spanish Naval Academy collaborators and the NPS Business School will provide insights into future directions of study. The analytical model will aid in determining the size and structure of the PCM linear system, and it will provide

information of the performance impact caused by varying the thermal properties of the system. The NPS Business School study will provide useful research into the economical restraints of the system. These restraints may prove to be the limiting factor to creating a PCM system which would be economically beneficial for the military. The results of both studies will need to be considered when determining the most beneficial direction for future research.

# APPENDIX. RELATED PUBLICATION

R. Agrawal, J. Hanna, I. E. Gunduz, and C. C. Luhrs. “Epoxy-PCM Composites with nanocarbons or multidimensional boron nitride as heat flow enhancers,” *Molecules*, vol. 24, (10), pp. 1883, May 2019.

The author contributed to this related work, an article that was published in May 2019 in *Molecules* as part of the journal’s special issue on phase change materials. The full article text may be read at https://www.mdpi.com/1420-3049/24/10/1883

THIS PAGE INTENTIONALLY LEFT BLANK

# LIST OF REFERENCES


[1] M. J. Lostumbo et al., “Overseas basing of U.S. military forces,” RAND Corp., Santa Monica, CA, USA, RR-201-NYCEDC, 2013. [Online]. Available: https://www.rand.org/content/dam/rand/pubs/research_reports/RR200/RR201/RAND_RR201.pdf

[2] J. Mattis, “Summary of the 2018 national defense strategy of the United States of America,” Washington, DC, USA, Jan. 2018.

[3] M. Galka, “Annual peak temperatures across the world.” 01 Aug. 2017. [Online]. Available: http://metrocosm.com/peak-temperature-map/. [Accessed: 30 Apr. 2019].

[4] “Baghdad min max temperature,” 2019. [Online]. Available: https://www.weatheronline.co.uk/weather/maps/city. [Accessed: 29 May 2019].

[5] “Phoenix min max temperature,” 2019. [Online]. Available: https://www.weatheronline.co.uk/weather/maps/city. [Accessed: 30 Apr. 2019].

[6] E. Malek, “Microclimate of a desert playa: evaluation of annual radiation, energy, and water budgets components,” *Int. J. Climatol*., vol. 23, no. 3, pp. 333–345, Mar. 2003.

[7] A. Sharma, V. , Tyagi, C. , Chen, and D. Buddhi, “Review on thermal energy storage with phase change materials and applications,” *Renew. Sust. Energ. Rev.*, vol. 13, no. 2, pp. 318–345, 2009.

[8] Z. Khan, Z. Khan, and A. Ghafoor, “A review of performance enhancement of PCM based latent heat storage system within the context of materials, thermal stability and compatibility,” *Renew. Sust. Energ. Rev*., vol. 115, pp. 132–158, May 2016.

[9] A. Pasupathy, R. Velraj, and R. . Seeniraj, “Phase change material-based building architecture for thermal management in residential and commercial establishments,” *Renew. Sust. Energ. Rev*., vol. 12, no. 1, pp. 39–64, 2008.

[10] C. Veerakumar and A. Sreekumar, “Phase change material based cold thermal energy storage: Materials, techniques and applications – A review,” *Int. J. Refrig*., vol. 67, pp. 271–289, Jul. 2016.

[11] J. I. Network, “Energy Storage: Phase Change Materials for Thermal Energy Storage.” [Online]. Available: https://www.climatetechwiki.org/technology/jiqweb-pcm-0. [Accessed: 15 Mar. 2019].

[12] K. Chintakrinda, R. D. Weinstein, and A. S. Fleischer, “A direct comparison of three different material enhancement methods on the transient thermal response of paraffin phase change material exposed to high heat fluxes,” *Int. J. Therm. Sci.*, vol. 50, no. 9, pp. 1639–1647, 2011

[13] M. E. Arce, M. A. A. Feijoo, A. S. Garcia, and C. C. Luhrs, “Novel Formulations of Phase Change Materials—Epoxy Composites for Thermal Energy Storage,” *Materials*, vol. 11, no. 2, p. 195, Jan. 2018.

[14] Y. Zhong et al., “Heat transfer enhancement of paraffin wax using compressed expanded natural graphite for thermal energy storage,” *Carbon*, vol. 48, no. 1, pp. 300–304, 2010.

[15] L. Fan and J. . Khodadadi, “Thermal conductivity enhancement of phase change materials for thermal energy storage: A review,” *Renew. Sust. Energ. Rev.*, vol. 15, no. 1, pp. 24–46, Jan. 2011.

[16] Y. Cui, C. Liu, S. Hu, and X. Yu, “The experimental exploration of carbon nanofiber and carbon nanotube additives on thermal behavior of phase change materials,” *Sol. Energy Mater. Sol. Cells.*, vol. 95, no. 4, pp. 1208–1212, 2011.

[17] J. Wang, H. Xie, and Z. Xin, “Thermal properties of paraffin based composites containing multi-walled carbon nanotubes,” *Thermochimica Acta*, vol. 488, no. 1, pp. 39–42, 2009.

[18] D. Kim, A. Kirakosyan, J. W. Lee, J.-R. Jeong, and J. Choi, “Flexible h-BN foam sheets for multifunctional electronic packaging materials with ultrahigh thermostability,” *Soft Matter*, vol. 14, no. 20, pp. 4204–4212, May 2018.

[19] C. Lin and Z. Rao, “Thermal conductivity enhancement of paraffin by adding boron nitride nanostructures: A molecular dynamics study,” *Appl. Therm. Eng.*, vol. 110, pp. 1411–1419, Jan. 2017.

[20] “Nonadecane.” [Online]. Available: https://pubchem.ncbi.nlm.nih.gov/compound/12401. [Accessed: 02 May 2019].

[21] “Eicosane.” [Online]. Available: https://pubchem.ncbi.nlm.nih.gov/compound/8222. [Accessed: 02 May 2019].

[22] “Epofix Cold-Setting Embedding Resin,” 2019. [Online]. Available: https://www.emsdiasum.com/microscopy/technical/datasheet/1232.aspx. [Accessed: 25 Mar. 2019].

[23] “Carbopol® 940 polymer,” 2019. [Online]. Available: https://www.lubrizol.com/Personal-Care/Products/Product-Finder/Products-Data/96. [Accessed: 10 May 2019].

[24] “Boron nitride, 255475.” [Online]. Available: https://www.sigmaaldrich.com/catalog/product/aldrich/255475?lang=en&region=US. [Accessed: 14 Apr. 2019].

[25] “Carbon nanofibers, 71980.” [Online]. Available: https://www.sigmaaldrich.com/catalog/product/aldrich/719803?lang=en&region=US. [Accessed: 14 Apr. 2019].

[26] “Carbon nanotube, multi-walled, 724769.” [Online]. Available: https://www.sigmaaldrich.com/catalog/product/aldrich/724769?lang=en&region=US. [Accessed: 14 Apr. 2019].

[27] R. Agrawal et al., “Epoxy-PCM Composites with nanocarbons or multidimensional boron nitride as heat flow enhancers,” *Molecules*, vol. 24, (10), pp. 1883, May 2019.

THIS PAGE INTENTIONALLY LEFT BLANK

# INITIAL DISTRIBUTION LIST

1. Defense Technical Information Center
   Ft. Belvoir, Virginia

2. Dudley Knox Library
   Naval Postgraduate School
   Monterey, California